**Role of a waste-derived polymeric biosurfactant in the sol–gel synthesis of nanocrystalline titanium dioxide**

UNIVERSITÀ DEGLI STUDI DI TORINO

# Role of a waste-derived polymeric biosurfactant in the sol-gel synthesis of nanocrystalline titanium dioxide

Vittorio Boffa,[a] Daniele G. Perrone,[b] Giuliana Magnacca[b,c,]* and Enzo Montoneri,[b]

[a]Aalborg University, Section of Chemistry, Shongaardsholmsvej 57, 9000 Aalborg, Denmark;

[b]Torino University, Dipartimento di Chimica, and [c]NIS Centre of Excellence, via Pietro Giuria 7, 10125 Torino, Italy.

*corresponding author: giuliana.magnacca@unito.it, ph.+39 011 670 7543, fax +39 011 7855

## Abstract

An inexpensive polymeric biosurfactant isolated from urban bio-wastes is shown to be a useful chemical aid in the synthesis of nanostructured materials with tunable pore size and surface hydrophilicity. Photocatalytic active $TiO_2$ powders were prepared by sol-gel reaction in the presence of variable amounts of a waste-derived polymeric biosurfactant. The products were characterized for morphology, crystal structures and surface hydrophilicity. The porosity data indicate that an increase of the biosurfactant amount in the reaction medium causes a decrease of pore size, pore volume and specific surface area in the synthesized oxide, whereas TEM and XRD data indicate that particle size decreases by increasing biosurfactant amount. These results suggest that biosurfactant molecules play a role in the nucleation step, during the formation of the titanium dioxide particles. The biosurfactant amount in the synthesis mixture affects also the hydrophilicity of titanium dioxide surface, as demonstrated by water-adsorption microcalorimetry measurements, but the results suggest that also this aspect is connected to crystal nucleation and growth during oxide formation.

Keywords: biosurfactants, structure-directing effect, titanium dioxide, urban waste, green sol-gel synthesis.

## 1. Introduction

Within the current trend to develop inexpensive and sustainable procedures for the fabrication of functional nanomaterials, various biological substances have been applied as tailoring agents for the preparation of nanostructured inorganic particles, monoliths and films [1-11]. The utilization of natural substances as structure directing agents is indeed attractive from several reasons: (i) they show specific reactivity; (ii) their anisotropy allows the fabrication of complex inorganic structure by facile synthetic procedures; (iii) they are renewable and often inexpensive ready-available materials.

Specific reviews [1,2] report various examples of bio-materials used as structure directing agents in the sol-gel synthesis of ceramic materials. For instance, silicon carbide cellular structures [3] have been obtained by infiltration of fuse silicon or of tetraethyl orthosilicate (TEOS) in a large variety of woods (oak, maple, beech, ebony, pine, poplar, etc. …) and other lignocellulosic supports [3-5]. Metal oxide fibers have been obtained via sol-gel process also in presence of cotton [6] or pure cellulose [7]. Starch has been applied in the preparation of titanium dioxide and silica monoliths having hierarchical porous structure [8,9]. Recently, yeast cells have been utilized as templating agents for the preparation of photoactive titanium oxide [10] and mesoporous zirconium phosphate [11] powders.

In this context, waste-derived biosurfactants (BSs) are interesting structure directing agents for the preparation of nanostructured materials, because of their green origin, inexpensiveness, and their ability to organize themselves in different supramolecular structures depending on composition, concentration and pH [12]. The origin, the extraction process, and the general structure of these biosurfactants are depicted in Fig. 1. Modern

cities create vast quantities of waste, which is collected and transported to dedicated treatment plants. In these facilities the organic fraction of the urban waste is typically stabilized by composting, i.e. an aerobic biodegradation process. The so obtained compost can be disposed in landfill areas or used as soil amendment, i.e. to improve soil physical properties, such as aeration and water retention. On the other hand, compost has been shown to contain large concentrations (up to 12 w%) of BSs, which can be easily isolated by extraction in alkali and precipitation at pH < 1.5. These BSs bear chemical similarity with soil organic matter [12,13] and might be exploited as valuable specialty chemicals. They are complex mixtures of polymeric molecules with average molecular weight ranging from $10^4$ to $10^6$ g $mol^{-1}$ and polydispersity index in between 6 and 60. These macromolecules contain several functional groups and C atoms of different polarity. They appear to be formed by flexible aliphatic chains substituted by aromatic rings and several functional groups as carboxilic acid (COOH), amide (CON), keto (C=O), phenol (PhOH), alkoxy (O-alkyl), anomeric carbon (O-C-O), and amines (NRR', with R and R' being alkyl or H) groups. At basic and neutral pH, negatively charged carboxylic acid groups guarantee biosurfactant solubility in water; whereas at low pH, carboxylic acids are in their protonated form and these waste-derived biosurfactants show scarce solubility. Simultaneous presence of hydrophobic aliphatic chains and acid moieties, as carboxylic acids and phenols, confers anionic surfactant-like behavior. Thus, BSs have been proposed as chemical auxiliaries for a broad spectrum of industrial and environmental applications, in substitution of the more expensive commercial synthetic surfactants, which are typically produced from oil-derived chemicals. BSs application spectrum encompasses detergency [14], textile dyeing [15,16], soil washing [16], photodegradation of organic pollutants in waste effluents [17,18]. The regional differences and the seasonal fluctuations in the

composition of organic waste might raise concern about BS reproducibility. However, it has been shown that BS structure, hydrophilicity and surfactant properties tends to level if the organic waste is treated for several days under aerobic conditions [19]. During the composting process, the organic components of the refuse are indeed metabolized by microorganisms, and BS structure becomes similar to the one of the humic substances present in surface water and soil.

The polyelectrolytic structure and the surfactant properties of BSs make them attractive chemical auxiliaries for the fabrication of nanostructure materials. Over the last three decades synthetic surfactants have been indeed largely applied as soft templates for the fabrication of inorganic materials with defined pore structure [20-22] or to stabilize (micro)emulsions for the synthesis of inorganic nanoparticles with well-defined size and shape [22-23]. A BS has been recently applied for the first time as sacrificial tailoring agents for the preparation of mesoporous silica powders [24] by sol-gel method. Fig. 2 shows the TEM picture of the silica particles prepared at a BS concentration of 3 g $L^{-1}$. This powder consisted of hollow spheres with ~ 4 nm large cavities. In the sample prepared at a BS concentration of 10 g $L^{-1}$ these particles were organized in large aggregates showing also interparticle pores with average size of about 30 nm. The advantages related to the use of BS as synthesis assisting agent, are twofold: to exclude expensive oil-based products from synthesis, and to add practical and economic meaning to the collection and recycling of wastes. Hence, the application of BSs to the synthesis of nanostructured materials is here extended to the preparation of $TiO_2$ powders, whose production has a highly practical relevance, in reason of the photocatalytical properties of this type of materials, e.g. in the remediation of aqueous effluents contaminated by organics [25-31]. Fabrication and morphological characterization of $TiO_2$ powders prepared

in the presence of a BS are discussed in this work. Furthermore, data on surface hydrophilicity are obtained to assess the capacity of the synthesized $TiO_2$ to interact with organic substrates, a basic property for a photocatalytic material. Even more important, this work aims to investigate if a BS can play a different role during nucleation and growth of silica and of titania particles, having silicon and transition metal ions a different coordination chemistry and thus a different sol-gel chemistry.

## 2. Materials and methods

### 2.1 Materials

Titanium tetraisopropoxide (TIIP, 97%), sodium hydroxide and concentrated hydrochloric acid (37%) were purchased by Aldrich. The bio-waste used as BS source was provided by A.C.S.R. s.p.a. (Borgo San Dalmazzo, CN, Italy). A 40/60 w/w mix of urban organic humid waste and park trimming residues was treated for 28 days in a cement pool by continuous air insufflation, daily turned up-side-down and finally sieved to 12 mm. A 0.5 Kg sample of this biomass was collected and used as biosurfactant source.

### 2.2 Biosurfactant isolation and characterization

A detailed description of isolation and characterization procedures of the BS substance used in this work, hereinafter referred to as CVU90, is given elsewhere [13,19]. The sourcing bio-waste was dispersed in water at a 1:4 w/v ratio. Solid NaOH tablets were added to the suspension to reach a NaOH/biomass w/w ratio of 0.02. The suspension was heated at 65 °C for 4 h. The resulting suspension was cooled to room temperature and centrifuged at 4000 rpm for 20 min. The supernatant solution was separated from the solid residue, which was washed repeatedly with distilled water until the supernatant liquid

phase was clear. All collected liquid fractions were mixed and acidified with 50% sulfuric acid to pH < 1.5. The precipitated BS fraction was separated by centrifugation as described above, washed with water until the final washing had pH of about 4 and dried in a vent oven at 105 °C for 1 day. The so obtained CVU90 was characterized by exclusion chromatography (SEC) coupled to on-line multi-angle laser light scattering (MALS), elemental analysis, potentiometric titration, $^{13}C$ NMR spectroscopy, and surface tension measurements, following a protocol specifically developed for this type of waste-derived organic substances [12].

### 2.3 $TiO_2$ synthesis

After dispersing CVU90 in deionized water, 30% w/w, aqueous NaOH was slowly added to the suspension until complete dissolution occurred and the solution pH was stable at 7. The solution was diluted with deionized water in a graduated flask to adjust the final CVU90 concentration to 50 g $L^{-1}$. An aliquot of the CVU90 solution was diluted with water in a graduated flask to obtain a concentration of 10 g $L^{-1}$. Titanium dioxide samples were prepared by dropping 2.83 ml of TIIP in 10 ml of the 50 g $L^{-1}$ and 10 g $L^{-1}$ CVU90 solutions. A third titanium dioxide sample was prepared by dropping 2.83 ml of TIIP in 10 ml of neat deionized water. Precipitation occurred as soon as TIIP was added to the solutions. The reaction mixtures were aged at 65 °C for 1 day. Afterwards the solid products were recovered by centrifugation, washed twice with 20 ml of water, and dried at 105 °C overnight. The powders were then calcined in air at 500 ºC for 3 hours (heating and cooling rate of 2 °C $min^{-1}$).

### 2.4 $TiO_2$ characterization

Specific surface area and porosity of materials were determined by means of $N_2$ adsorption at liquid-nitrogen boiling point in a gas-volumetric apparatus (ASAP2020 model by Micromeritics). Samples were outgassed at 300 ºC in vacuum (residual pressure $10^{-2}$ mbar) until no gaseous species arise from them (about 4 hours). Specific surface areas were determined using the Brunauer-Emmett-Teller (BET) model [32] and porosity was obtained applying the Barrett-Joyner-Halenda (BJH) method on desorption branch of the isotherms [33]. Crystal structure of materials was determined using X-ray diffractometer Philips PW1830 working with Co-Kα source and Bragg-Brentano geometry. BS effects during synthesis on $TiO_2$ crystallites domain size (Dv, in the following), was evaluated. A lower limit value of Dv was calculated employing the Scherrer equation relating the size of sub-micrometre particles in a solid to the broadening of diffraction pattern main peaks [34] and considering k = 0.9 as the shape factor and λ = 1.789010 Å as the wavelength of the X-rays for Co Kα1 radiation. High-resolution transmission electron microscopy (HRTEM) images were obtained with a JEOL 3010-UHR instrument (acceleration potential: 300 kV). Samples for TEM investigation were supported onto holed carbon coated copper grid by dry deposition. The surface hydrophilicity of the prepared $TiO_2$ powders was evaluated according to a previously reported procedure [35,36] using an adsorption microcalorimetry (Tian-Calvet model by Setaram) equipped with a gas-volumetric apparatus for the quantitative and energetic study of surface-water interaction.

Codice campo modificato

Codice campo modificato

Codice campo modificato

Codice campo modificato

## 3. Results

### 3.1. Biosurfactant structure

As shown in Fig. 3, CVU90 has a broad molecular mass distribution over the $10^3$-$10^6$ g $mol^{-1}$ range with a maximum at 3 $10^3$ g $mol^{-1}$. Average mass in weight ($M_W$) and number

($M_N$) of 7.1 $10^3$ and 1.7 $10^5$ g $mol^{-1}$ were respectively calculated from this distribution, corresponding to a polydispersity index ($M_W/M_N$) of 23. Such a polydispersity is not surprising, considering that similarly to other waste-derived BSs [13], CVU90 bears a highly complex macromolecular structure. Functional group distribution of CVU90 is reported in Table 1. Since the characterization protocol used for the acquiring these data is based on combining potentiometric titration, elemental analysis, and $^{13}C$ NMR data, the concentration of the functional groups is here expressed as milliequivalent of carbon atoms per gram of dry matter. These analytical data were used to draw the virtual molecular fragment of CVU90, which is depicted in Fig. 4. This fragment consists of hydrophobic alkyl chains and hydrophilic acidic moieties, namely carboxylic acids and phenolic groups: this confirms the surfactant-like behavior of CVU90. At 25 ºC and pH 7 a virtual critical micellar concentration (cmc) of 2.0 g $L^{-1}$ was measured for CVU90 [19]. At this concentration the water surface tension is lowered from 71.2 mN $m^{-1}$ (net water) to 31.4 mN $m^{-1}$, which confirms the good surfactant properties of the investigated BS. From previous results [24], BSs are expected to effectively act as templating agents only when used at concentration well above their virtual cmc. For this reason, in this study CVU90 was used at concentrations equal to 5 and 25 times its virtual cmc.

### 3.2 $TiO_2$ structure and morphology

Three $TiO_2$ powders were prepared by hydrolysis and condensation of TIIP in acid-catalyzed conditions, at a different biosurfactant concentration, namely 0.0 g $L^{-1}$ (T00), 10 g $L^{-1}$ (T10), and 50 g $L^{-1}$ (T50). Table 2 summarizes the experimental data for the preparation of the titanium dioxide powders and physical data extrapolated from XRD and gas-volumetric analyses. X-ray diffractograms of the three powders are reported in Fig. 5.

All XRD patterns evidence the presence of titanium dioxide anatase phase. However, the sample prepared in the absence of CVU90 shows also two weak signals at $2\theta = 36°$ and 59°, corresponding to the most intense diffraction peaks of the brookite phase. The three diffractograms show crystal peaks characterized by large width. According to Scherrer equation [34], the degree of crystallinity of the three powders is compatible with materials consisting of nanometric crystalline particles. Moreover, the width of peaks increases with the amount of BS used in the synthesis of the materials, indicating that the size of these crystallites decreases ($D_v$ values are reported in Table 2) by increasing BS concentration.

Fig. 6 shows the TEM pictures taken on samples T00 and T50. As suggested by XRD analysis, the powders consist of nano-crystals and the crystallite size of the sample T50 (prepared with CVU90) is significantly smaller than that of sample T00 (prepared without CVU90). Both of them have polyhedral shape and their size is about 20 nm and 10 nm, respectively, in quite good agreement with Scherrer determinations reported in Table 2. Sample T00 is made of crystalline particles (as evidenced by the presence of interference fringes) almost irregular in shape, with average size of ca. 20 nm and arranged in large aggregates. The particles do not seem to have intrinsic porosity, as observed analyzing the high resolution image reported in Fig. 6B; but particles aggregates form quite large interparticle pores, as evidenced in Fig. 6A by yellow arrows. The analysis of interference fringe patterns of the TEM picture in Fig. 6B confirms the presence of anatase phase, evidenced by the signal $d_{hkl}$=3.50 Å relative to anatase (101) plane, and of brookite phase, due to the signals of $d_{hkl}$=2.26 and 2.40 Å possibly related to brookite (022) and (210) planes, respectively. Sample T50 is made of small crystalline particles of ca. 10 nm of width, extensively aggregated. Also in this case the particles appear to be dense crystallites and the porosity of the material is due to interparticle aggregation. The analysis of

interference fringe patterns evidences the principal presence of anatase phase, $d_{hkl}$=3.50 Å, plane (101). The signals of $d_{hkl}$=2.14 Å, assignable to (212) and (104) planes of brookite phase, are also visible for a few crystallites in some TEM pictures. Nevertheless, the concentration of brookite is expected to be rather low since it was not detected by XRD analysis.

Fig. 7 reports adsorption/desorption isotherms and BJH pore size distribution curves relative to T10, T50 and T00 reference systems. T00 sample presents an isotherm typical of mesoporous materials, characterized by the presence of a hysteresis loop in a range of $N_2$ relative pressure between 0.8 and 1. By comparison, the hysteresis loops for the T10 and T50 samples are narrower and start at lower $N_2$ pressure, i.e. at ~ 0.7 in the case of T10 and at ~ 0.60 in the case of T50. These features are consistent with the porosity data reported in Table 2, which show lower pore volume and pore size in $TiO_2$ system upon increasing CVU90 concentration in the sample preparation medium. Indeed, T00 sample shows a quite narrow BJH porosity distribution centered at about 20 nm of pore width, whereas the T10 and T50 samples exhibit wider pore size distributions centered at 10 and 7 nm of pore width respectively. Consequently, the cumulative pore volume decreases from 0.45 $cm^3\ g^{-1}$ for T00 to 0.30 to 0.19 $cm^3\ g^{-1}$ for the T10 and T50 samples, respectively. These results are consistent with the TEM pictures and the XRD data: samples with higher BS concentration consist of smaller $TiO_2$ particles, and thus inter-particle pores are also smaller. On the other hand, a smaller particle size should result in a higher specific surface area (SSA). However, the data in Table 2 show the opposite trend, being T50 the sample with the smallest $D_v$ and the lowest SSA. This apparently odd feature will be discussed in the next section, after considering the results of the microcalorimetric analysis.

### 3.3 $TiO_2$ hydrophilicity

Considering the possible application of the synthesized $TiO_2$ powders as photocatalysts for the removal of organic pollutants from aqueous effluents, their surface hydrophilicity was measured to obtain evidence on the capacity of these materials to interact with polar and apolar substances eventually dispersed in water. The surface hydrophilicity measurements were carried out following water adsorption at 30°C on samples vacuum-activated at 30°C according to a previously reported method [35,36]. The procedure consists in studying the interaction between water and the surface of the solid material under investigation by an adsorption microcalorimeter equipped with a gas-volumetric apparatus. This allows determining both the amount of water adsorbed on the material surface and the energy released brought by the type of interaction, i.e., in the order of decreasing energy, specific chemisorption of water molecule on adsorbing sites and physisorption of water molecules by H-bonds formation. The 44 kJ $mol^{-1}$ liquefaction enthalpy of water vapor is taken as threshold between hydrophilic and hydrophobic systems: i.e., interactions involving energies higher than 44 kJ $mol^{-1}$ are due to hydrophilic surfaces, whereas energies lower than 44 kJ $mol^{-1}$ derive from hydrophobic surfaces.

The results of these measurements for T00 and T50 samples are reported in Fig. 8A, B and C. The experimental points were collected for water vapor pressure values at the equilibrium ($p_e$) smaller than 4 mbar, in order to examine only the interactions due to the first layer of water molecules formed at the surface of materials (this way the interactions due to multiple layers formation and liquefaction of vapor are not considered). The first plot shows that from about 0.7 mbar of $p_e$ the amount of water adsorbed per unit surface by the T50 sample is higher than that observed for T00 sample. These data imply that the number of adsorbing sites available for interaction with water molecules in the T50 sample

(ionic sites and/or OH groups) is higher than those available at T00 surface. Fig. 8B reports the heat of adsorption ($Q_{int}$) as a function of $p_e$. Also in this case, the relative position of the two curves indicates that T50, possessing a larger number of adsorbing sites with respect to T00 sample, evolves higher cumulative energies in the interaction with water. It is also possible to quantify the molar heat ($q_{ads}$) evolved for each dose of water contacted with materials surface. In this case, the interaction energies related to the adsorbed amount, calculated dose by dose, and reported as function of coverage, allow to figure out the molar energies of water-surface interaction. The extrapolated $q_{ads}$ curves are reported in Fig. 8C. The shape of the adsorption curves relative to both samples is typical of heterogeneous surfaces, involving various types of interactions. In essence, the first water molecules interact with surface evolving energies as high as 250 kJ $mol^{-1}$, with almost no differences observable for the two samples. Further water molecules are physisorbed reaching a plateau of energy at about 80 kJ $mol^{-1}$ for T00 and about 60 kJ $mol^{-1}$ for T50. All the measured values are higher than 44 kJ $mol^{-1}$, indicating that all samples are hydrophilic and can efficiently interact as photocatalyst with hydrophilic substrates. Nevertheless, it is noteworthy that T50 sample shows lower interaction energies at high coverage with respect to T00 sample. That suggests that T50 does not possess a stronger interaction with water in terms of energy but possesses a wider number of adsorbing sites with respect to T00 sample, as actually indicated by the curves in Fig.8A.

## 4. Discussion

BSs have a complex macromolecular structure. In reason of the presence of polar moieties as carboxylic acids, phenols, and amines, these substances can act as surfactants, polyelectrolites or chelating agents. Thus, the presence of a BS in the reaction mixture can

influence the formation of the oxidic material during sol-gel synthesis in different ways. Surfactant micelles are typically used as templates to control the pore size and shape of sol-gel derived oxide materials: in this case, the final consolidate oxide material retains size and connectivity of the surfactant micelles in the reaction mixture. This seems to be the case of the silica particles in Fig. 2, which were prepared by hydrolysis and condensation of tetraethyl orthosilicate (TEOS) in presence of a BS as pore tailoring agent. These particles indeed have a few nanometer large cavities whose size is compatible with that of BS micelles or aggregates, removed by calcination. This consideration is supported by the fact that, as depicted in Fig. 9, both pore volume and pore size of the final silica particle increased by raising the biosurfactant concentration in the synthetic mixture from 0.3 to 10 g $L^{-1}$.

On the contrary, Fig. 9 shows that T00, T10 and T50 powders had progressively smaller pore size and cumulative pore volume. Thus, the data presented in this paper suggest that BSs play a different role when used as tailoring agent in the presence of a titanium alkoxide (namely, titanium tetraisopropoxide). Recently, He et al. [10] reported the use of yeast cells as templating agent for the synthesis of a photoactive $TiO_2$ powder. During fermentation yeast cells produced macromolecules with surfactant properties including proteins and polysaccharides. Anionic hydrophilic groups on these macromolecules (mainly $-COO^-$ and $-OPO_3^{2-}$) provided oriented nucleation sites for the positively charged $Ti^{4+}$ ions during the sol synthesis. The resulting material showed crystal size of about 10 nm and a bimodal pore size distribution with maxima at about 5 and 11 nm. This mechanism is well compatible with the characteristic of BS molecules and with the morphology of the final consolidated $TiO_2$ powders here studied. Indeed, Gigant et al. [37] has reported that phenolic compounds, namely pyrocatechol, salicylic acid, and 2,2'-

biphenol, form relatively stable polynuclear complexes with $Ti^{4+}$ ions, generated by hydrolysis of titanium(IV) butoxide. Therefore, it is well possible that titanium (IV) complexes, as the one reported in Fig. 10, were formed just after addition and subsequent hydrolysis of TIIP in the CVU90 solution. These titanium (IV) complexes act as nucleation sites, around which $TiO_2$ nanoparticles grow by condensation of the dissolved monomers and $TiO_2$ clusters. Therefore, an increase of CVU90 concentration in the reaction mixture is expected to lead the formation of a larger number of nucleation centers and thus to a larger number of $TiO_2$ nanoparticles with a smaller size. Indeed, the larger is the amount of hydrolyzed TIIP will be consumed for nuclei formation, the lower will be the amount of hydrolyzed TIIP available for particles growth by means of condensation reaction. This mechanism is compatible with the experimental evidences presented in this study. In fact, an increase of CVU90 in the reaction mixture leads to the formation of $TiO_2$ crystals with smaller size.

Moreover, the presence of CVU90 in the reaction mixture has a not negligible influence on the hydrophilicity of the final oxide materials. The microcalorimetric results indicate that T50 sample possesses a larger number of water adsorbing sites with respect to T00 sample (see Fig.8A, with data normalized to the specific surface area of the materials). This indicates that BS used during oxide preparation causes an increase of the number of adsorbing sites for $m^2$ of sample. Considering the $q_{ads}$ curves reported in Fig.8C, it is possible to observe that the larger difference shown by T00 and T50 samples forms at high coverage, when the interaction energies measured is in the range 60-80 kJ $mol^{-1}$, i.e. when water molecules interact with OH groups forming H-bonds. That implies that the number of OH groups in T50 sample is higher than in T00 one. In some extent this confirms that, in the presence of BS, a larger amount of TIIP is consumed to form nucleation centers,

whereas a minor amount is consumed for particles growth by condensation reaction leading to a higher number of OH groups retained at the surface of material. This has two implications. The first one concerns the kind of hydrophilicity obtained in BS presence: as already discussed, the hydrophilicity of T50 sample is induced by a large number of OH groups and is not due to the presence of uncoordinated OH groups giving high interaction energies with water. The latter implication concerns the aggregation extent and, consequently, area and porosity of the materials: the larger the aggregation induced by a large number of OH groups (T50 sample), the lower the specific surface area and porosity of corresponding material.

## 5. Conclusions

The role of a waste derived polymeric biosurfactant (BS, namely CVU90) in the formation of titanium dioxide particles by sol-gel synthesis was investigated for the first time. The scope of this work was dual: (i) to fabricate novel $TiO_2$-based materials via a sustainable synthesis excluding oil-based intermediates and (ii) investigate the effect of a BS on the nucleation, growth and consolidation of titanium dioxide particles. XRD and TEM data indicated that BS acted as structure directing agent. Titanium dioxide crystals obtained in the presence of BS were smaller with respect to the sample synthesized without biosurfactant. The presence of BS hampered the formation of brookite phase, which was not detected in the T10 and T50 samples by XRD analysis. The presence of BS led also to the formation of a larger number of surface hydroxyls. Ti-OH groups induced a good hydrophilicity to the two titania samples studied, but the hydrophilicity shown by T50 sample is essentially due to the presence of many OH groups, whereas is almost limited in

terms of OH-water interaction energies. The interaction among Ti-OH groups facilitated aggregation of the primary titania particles and thus hydroxyl density influenced interparticle porosity. Therefore, T50 particles which have higher hydroxyl density, reasonably showed higher aggregation (TEM analysis) and thus lower pore volume and surface area (porosimetry measurements) than T00.

Comparing these results with those obtained for the synthesis of silica particles, it was possible to observe that the waste derived anionic biosurfactant plays a different role when used in the presence of TEOS or TIIP. This can be explained by considering the different coordination chemistry of silicon and titanium (and transition metal in general): $Ti^{4+}$ ions have indeed empty *3d* orbitals and thus are prone to interact with Lewis bases, as the oxygen-containing moieties of the waste-derived biosurfactant.

Further extension of this work will concern the study of the photocatalytic properties of the synthetized materials in relation of their morphology and surface properties.

## Ackowledgements

The Authors wish to thank the European Union for supporting this research (project PIRSESGA2010269128, EnvironBOS).

## References

1. T.X. Fan, S.K Chow, D. Zhang, Biomorphic mineralization: from biology to materials, Progress in Materials Science, 54 (2009) 542-659.
2. S.R. Hall, Biotemplated syntheses of anisotropic nanoparticles, Proceedings of the Royal Society A, 465 (2009) 335-366.
3. P. Greil, Biomorphous ceramics from lignocellulosics, Journal of the European

Ceramic Society, 21 (2001) 105-118.

4. D. Shao, X. Wang, Q. Fan, Photocatalytic reduction of Cr(VI) to Cr(III) in solution containing ZnO or ZSM-5 zeolite using oxalate as model organic compound in environment, Microporous and Mesoporous Materials, 117 (2009) 243-248.
5. A. Zampieri, S. Kullmann, T. Selvam, J. Bauer, W. Schwieger, H. Sieber, T. Fey, P. Greil, Bioinspired rattan-derived sisic/zeolite monoliths: preparation and characterisation, Microporous and Mesoporous Materials, 90 (2006) 162-174.
6. T. Fan, B. Sun, J. Gu, D. Zhang, L.W.M. Lau, Biomorphic $Al_2O_3$ fibers synthesized using cotton as bio-templates, Scripta Materialia, 53 (2005) 893-897.
7. N. S. Venkataramanan, K. Matsui, H. Kawanami, Y. Ikushima, Green synthesis of titanium dioxide nanowire composites on natural cellulose fibers, Green Chemistry, 9 (2007) 18-19.
8. Z. Miao, K. Ding, T. Wu, Z. Liu, B. Han, G. An, S. Miaz, G. Yang, Fabrication of 3D-networks of native starch and their application to produce porous inorganic oxide networks through a supercritical route, Microporous and Mesoporous Materials, 111 (2008) 104-109.
9. Y. Zhang, L. Hu, J. Han, Z. Jiang and Y. Zhou, Soluble starch scaffolds with uniaxial aligned channel structure for in situ synthesis of hierarchically porous silica ceramics," Microporous and Mesoporous Materials, 130 (2010) 327-332.
10. W. He, J. Cui, Y. Yue, X. Zhang, X. Xia, H. Liu and S. Lui, High-performance $TiO_2$ from Baker's yeast, Journal of Colloid and Interface Science, 354 (2011) 109-115.
11. X. Tian, W. He, J. Cui, X. Zhang, W. Zhou, S. Yan, X. Sun, X. Han, S. Han, Y. Yue, Mesoporous zirconium phosphate from yeast biotemplate, Journal of Colloid and Interface Science, 343 (2010) 344-349.

12. E. Montoneri, V. Boffa, P. Savarino, D. G. Perrone, G. Musso, R. Mendichi, M. R. Chierotti, R. Gobetto, Biosurfactants from Urban Green Waste, ChemSusChem, 2, (2009) 239–247.
13. E. Montoneri, V. Boffa, P. Savarino, D. G. Perrone, M. Ghezzo, C. Montoneri, Acid soluble bio-organic substances isolated from urban bio-waste. Chemical composition and properties of products, Waste Management, 31 (2011) 10-17.
14. P. Savarino, E. Montoneri, G. Musso, V. Boffa, Biosurfactants from urban wastes for detergent formulation: surface activity and washing performance, Journal of Surfactants Detergents, 13 (2010) 59-68.
15. P. Savarino, E. Montoneri, S. Bottigliengo, V. Boffa, T. Guazzetti, D.G. Perrone and R. Mendichi, Biosurfactants from urban wastes as auxiliaries for textile dyeing, Industrial & Engineer Chemical Research, 48 (2009) 3738-3748.
16. E. Montoneri, V. Boffa, P. Savarino, F. Tambone, F. Adani, L. Micheletti, C. Gianotti, R. Chiono, Use of biosurfactants from urban wastes compost in textile dyeing and soil remediation, Waste Management, 29 (2009) 383-389.
17. A. Bianco Prevot, D. Fabbri, E. Pramauro, C. Baiocchi, C. Medana, E. Montoneri, V. Boffa, Sensitizing effect of bio-based chemicals from urban wastes on the photodegradation of azo-dyes, Journal of Photochemistry and Photobiolology A, 209 (2010) 224-231.
18. A. Bianco Prevot, P. Avetta, D. Fabbri, E. Laurenti, T. Marchis, D.G. Perrone, E. Montoneri, V. Boffa, Waste-derived bioorganic substances for light-induced generation of reactive oxygenated species, ChemSusChem, 4 (2011) 85-90.
19. E. Montoneri, V. Boffa, P. Savarino, D.G. Perrone, C. Montoneri, R. Mendichi, J. Acosta, S. Kiran, Behavior and properties in aqueous solution of biopolymers isolated

from urban refuse, Biomacromolecules, 11 (2010) 3036–304.

20. L. Han, S.N. Che, Anionic surfactant templated mesoporous silicas (AMSs), Chemical Society Reviews, 42 (2013) 3740-3752.

21. A.E.C. Palmqvist, Synthesis of ordered mesoporous materials using surfactant liquid crystals or micellar solutions, Current Opinion in Colloid and Interface Science, 8 (2003) 145-155.

22. V.T. John, Blake Simmons, G. L. McPhersonb, Arijit Bosec Recent developments in materials synthesis in surfactant systems, Current Opinion in Colloid and Interface Science 7 (2002) 288-295.

23. R.T. Ren, Z.Y. Yuan, B.L. Su, Surfactant-assisted preparation of hollow microspheres of mesoporous $TiO_2$ Chemical Physics Letters, 374 (2003) 170-175.

24. V. Boffa, D. G. Perrone, E. Montoneri, G. Magnacca, L. Bertinetti, L. Garlasco, R. Mendichi, A waste derived biosurfactant for preparation of templated silica powders, ChemSusChem, 3 (2010) 445-452.

25. C. Chen, W. Ma, J. Zhao, Semiconductor-mediated photodegradation of pollutants under visible-light irradiation, Chemical Society Reviews, 39 (2010) 4206-4219.

26. T. Sivlim, T; S. Akkan, I. Altin, M. Koc, M. Sökmen, $TiO_2$ immobilized biodegradable polymer for photocatalytic removal of chlorophenol, Water Air And Soil Pollution, 223 (2012) 3955-3964.

27. N. R. Khalid, E. Ahmed, Z. Hong, Y. Zhang, M. Ullah, M. Ahmed, Graphene modified Nd/$TiO_2$ photocatalyst for methyl orange degradation under visible light irradiation. Ceramics International, 39 (2013) 3569-3575.

28. H. Meng, B. Wang, S. Liu, R. Jiang, H. Long, Hydrothermal preparation, characterization and photocatalytic activity of $TiO_2$/Fe–$TiO_2$ composite catalysts,

Ceramics International, 39 (2013) 5785-5793.

29. X. Wei, H. Wang, G. Zhu, J. Chen, Li. Zhu, Iron-doped $TiO_2$ nanotubes with high photocatalytic activity under visible light synthesized by an ultrasonic-assisted sol-hydrothermal method, Ceramics International, 39 (2013) 4009-4016.
30. B. Aysin, A. Ozturk, J. Park, Silver-loaded $TiO_2$ powders prepared through mechanical ball milling, Ceramics International, 39 (2013) 7119-7126.
31. I Altin, M. Sökmen, Preparation of $TiO_2$-polystyrene photocatalyst from waste material and its usability for removal of various pollutants, Applied Catalysis B: Environmental, 144 (2014) 694-701.
32. S. Brunauer, P.H. Emmett, E. Teller, Adsorption of Gases in Multimolecular Layers, Journal of the American Chemical Society, 60 (1938) 309.
33. E. P. Barrett, L. G. Joyner and P. P. Halenda, The determination of pore volume and area distributions in porous substances. I. Computations from nitrogen isotherms, Journal of the American Chemical Society, 73 (1951) 373-380.
34. P. Scherrer, Nachr. Ges. Wiss. Giittingen 96 (1918).
35. A. Cauvel, D. Brunel, F. Di Renzo, E. Garrone, B. Fubini, Hydrophobic and Hydrophilic Behavior of Micelle-Templated Mesoporous Silica, Langmuir, 13 (1997) 2773-2778.
36. B., Bonelli, B. Onida, J. D. Chen, A. Galarneau, F. Di Renzo, F. Fajula, B. Fubini, E. Garrone, Characterisation of Al-rich microporous micelle-templated silicates. Part II: Spectroscopic and microcalorimetric study of the accessibility of exchanged alkali-cations to carbon dioxide, Microporous and Mesoporous Materials, 87 (2006) 170-176.
37. K. Gigant, A. Rammal, M. Henry, Synthesis and molecular structures of some new

Titanium (IV) aryloxides, J. Am. Chem. Soc., 123 (2001) 11632-11637.

**FIGURE CAPTIONS**

Fig.1: Source and process steps for the extraction of a waste derived biosurfactant (BS). The chemical structure represents a hypothetical BS fragment.

Fig.2: Silica nanoparticles prepared by hydrolysis and condensation of tetraethyl orthosilicate (TEOS) in the presence of a waste-derived biosurfactant (3 g $L^{-1}$)

Fig.3: CVU90 molecular mass distribution.

Fig.4: Virtual molecular fragments for CVU90 fitting analytical data reported in Table 1. H atoms bonded to C atoms are omitted; sinusoidal bold lines indicate other molecular fragments.

Fig.5: XRD data for titanium dioxide samples prepared in the absence (pattern a) and in the presence of CVU90 at 10 g $L^{-1}$ (pattern b) and 50 g $L^{-1}$ (pattern c). The arrows indicate the principal signals of titanium dioxide brookite phase. The curves were shifted for the sake of clearness; the marker within the figure corresponds to the ordinate value of 200 cps.

Fig.6: TEM pictures of the samples T00 (A and B) and T50 (C). Yellow arrows evidence the presence of interparticle porosity. In section B (high resolution image of T00 sample) the principal interference fringe patterns are evidenced.

Fig.7: $N_2$ adsorption isotherms at -196°C (A) and BJH pore size distribution (B) for samples T00 (triangles), T10 (squares) and T50 (circles). Empty symbols refer to adsorption branch, black symbols refer to desorption branch. The curves reported in Fig. 7A are shifted for the sake of clearness.

Fig.8: Water adsorption on T00 (triangles) and T50 (circles). Section A: adsorbed amount reported vs. equilibrium pressure. Section B: heats of adsorption ($Q_{ads}$) vs. equilibrium pressure. Section C: heats of adsorption evolved dose by dose ($q_{ads}$) vs. coverage. The dotted line indicates the reference value of 44 kJ $mol^{-1}$ (liquefaction enthalpy of water

vapor).

Fig.9: Pore volume (a) and average pore size (b) of $SiO_2$ and $TiO_2$ powders obtained by the sol-gel method in the presence of different concentration of a waste-derived biosurfactant (BS).

Fig.10: Possible coordination modes of a virtual salicylic acid-like unit on a CVU90 fragment and titanium (IV) ions. Titanium (IV) and oxygen ions are indicated by black and gray circles, respectively. The salicylic acid-like unit can coordinate one or more titanium (IV) ions [37].

Table 1. Concentration of functional groups in CVU90 [13] expressed as milliequivalent of carbon atoms per gram of dry matter (meq C /g).

| Functional group | [meq C /g] |
|---|---|
| Aliphatic | 10.3 |
| Aromatic | 4.3 |
| Phenoxi (*Ph-OR*) | 1.4 |
| Phenolic (*Ph-OH*) | 0.7 |
| Alkoxy (*C-O*) | 3.5 |
| Anomeric (*O-C-O*) | 1.0 |
| Ketonic (*C=O*) | 0.8 |
| Carboxylic (*COOH*) | 2.0 |
| Amides (*CON*) | 1.6 |
| Amines (*C-N*) | 1.2 |

Table 2. Experimental conditions for the preparation of $TiO_2$ samples and characterization data by XRD, namely crystallographic phases (A=anatase and B=brookite) and particle size ($D_v$), and $N_2$ adsorption analyses, namely specific surface area (SSA), average pore sizes (curve maxima) and pore volume.

| | **Preparation** | | **XRD** | | **$N_2$ adsorption analysis (T=-196°C)** | | |
|---|---|---|---|---|---|---|---|
| *Sample* | *$BS/TiO_2$ w/w* | *Calcination T [°C]* | *Crystallographic phases* | *$D_v$ (nm )* | *SSA ($m^2 g^{-1}$)* | *Average Pore size (nm)* | *Pore volume ($cm^3 g^{-1}$)* |
| *T00* | 0 | 500 | A + B | 18.0 | 88 | 21 and 2 | 0.45 |
| *T10* | 0.13 | 500 | A | 10.5 | 80 | 10 and 2 | 0.30 |
| *T50* | 0.66 | 500 | A | 10.0 | 69 | 7 and 2 | 0.19 |

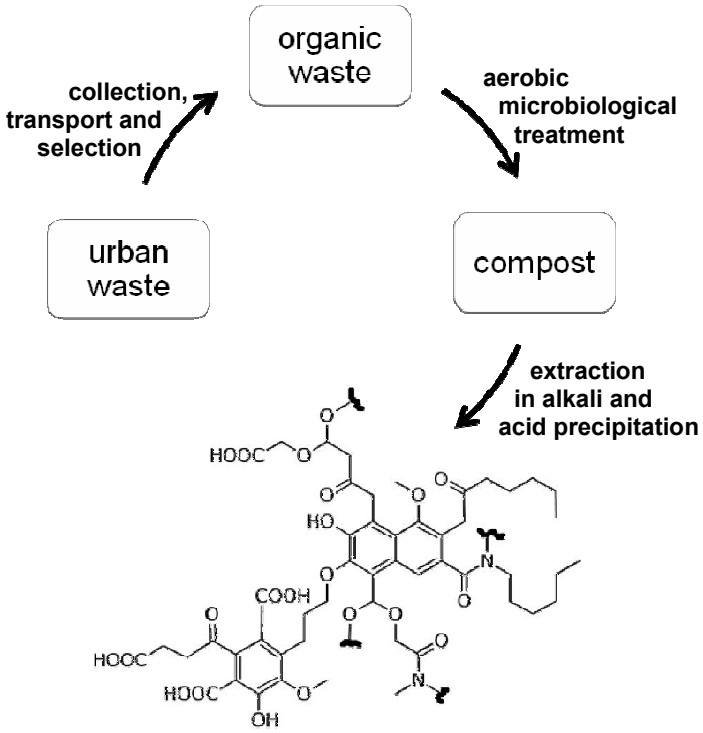
organic waste
aerobic microbiological treatment
compost
extraction in alkali and acid precipitation
urban waste
collection, transport and selection
Waste derived biosurfactant (BS)

Fig. 1.

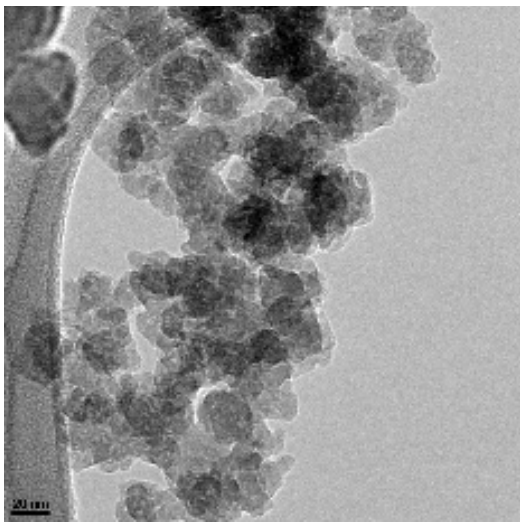

Fig. 2.

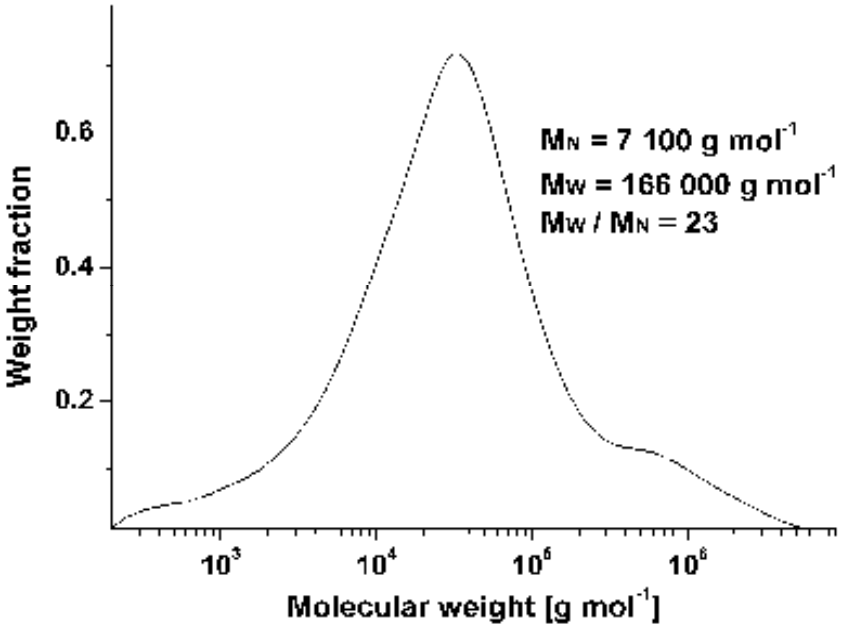
Weight fraction
0.6
0.4
0.2
$M_N$ = 7 100 g mol$^{-1}$
Mw = 166 000 g mol$^{-1}$
Mw / $M_N$ = 23
$10^3$
$10^4$
$10^5$
$10^6$
Molecular weight [g mol$^{-1}$]

Fig. 3.

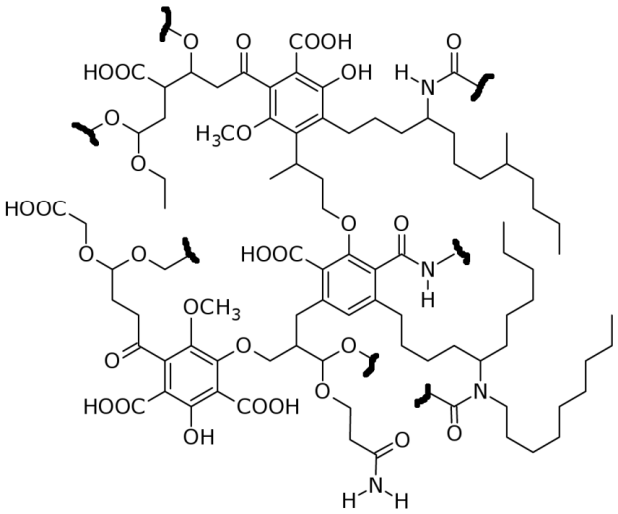
HOOC
O
O
COOH
OH
H
N
O
H3CO
HOOC
O
O
HOOC
O
O
N
H
OCH3
O
O
O
O
HOOC
COOH
OH
O
N
O
O
N
H
H

Fig. 4.

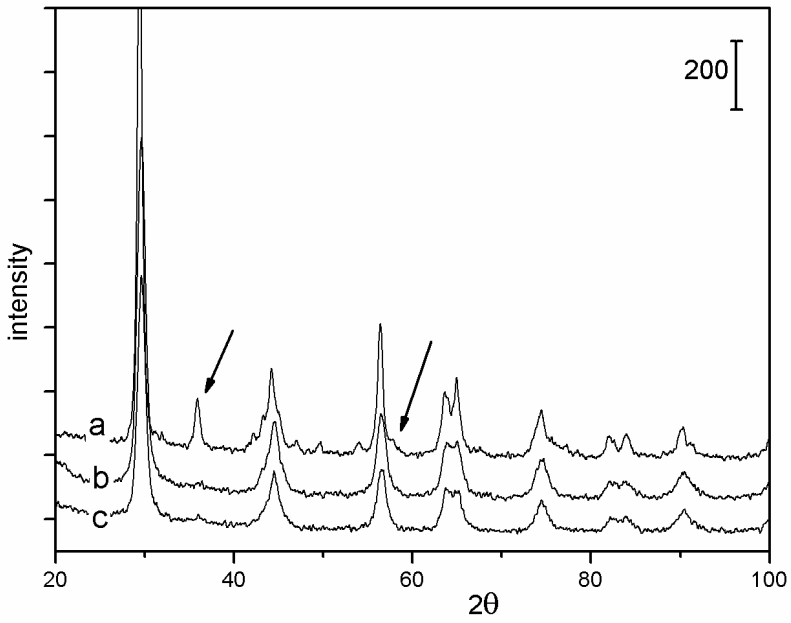


Fig. 5.

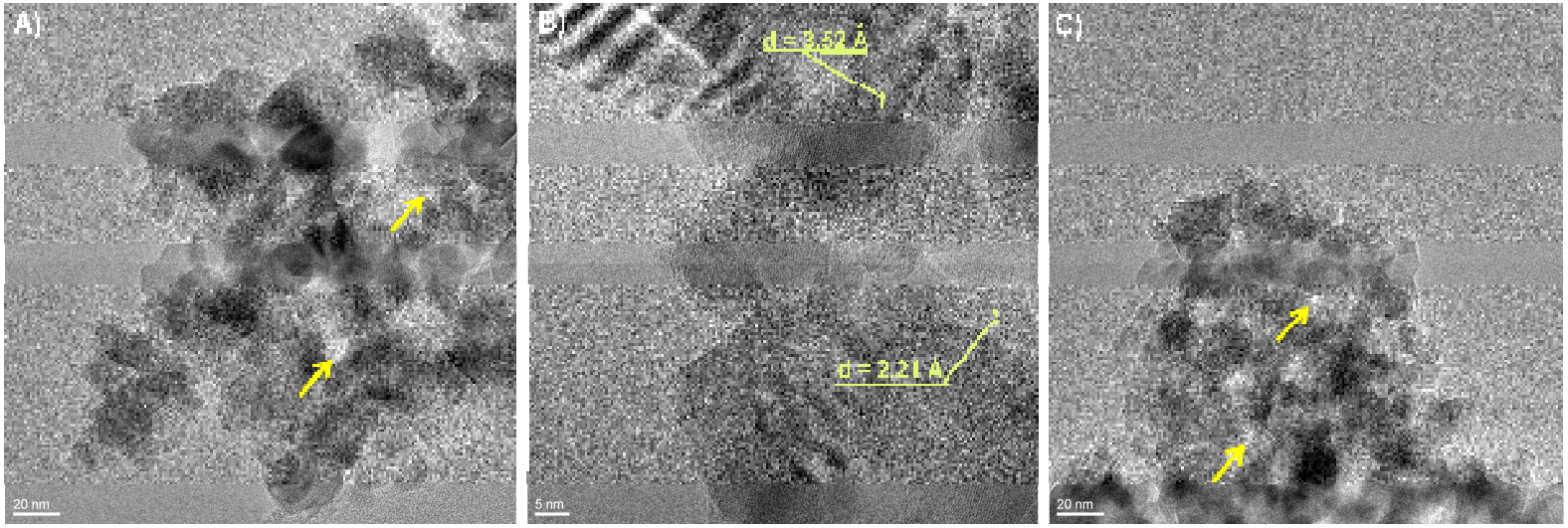


Fig. 6.

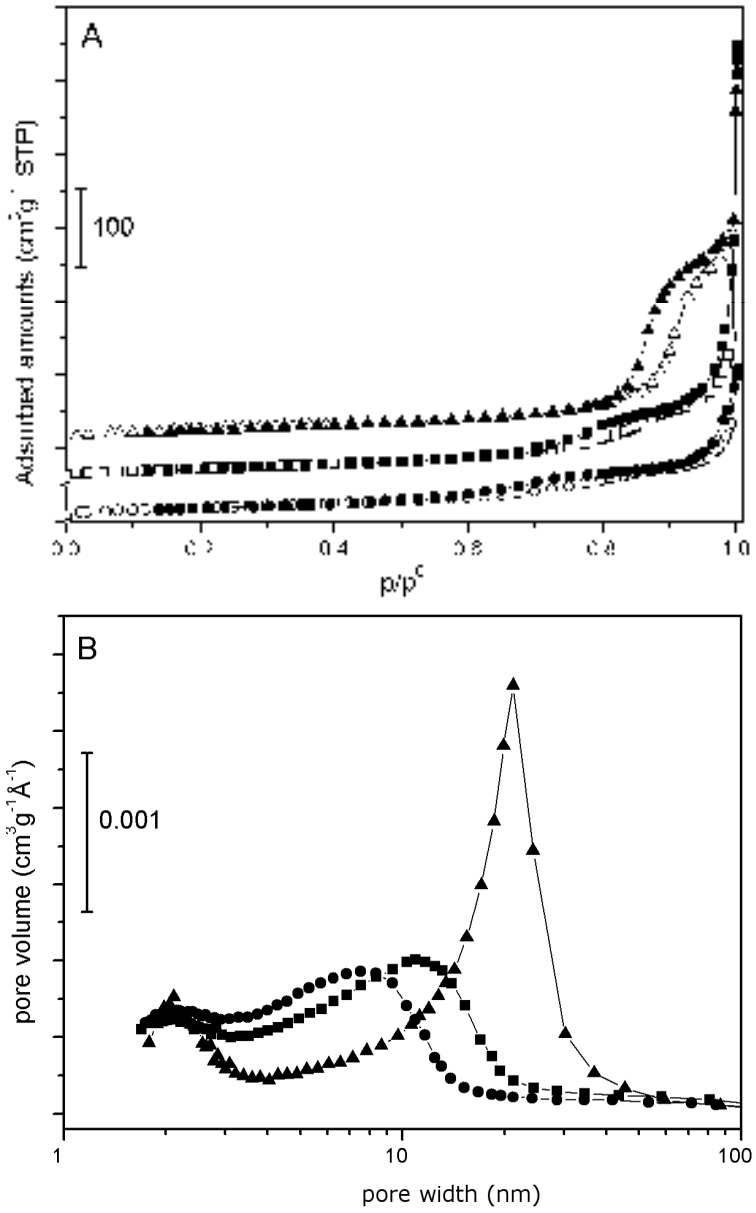
A
100
Adsorbed amounts (cm³g⁻¹ STP)
p/p°
B
0.001
pore volume (cm³g⁻¹Å⁻¹)
1
10
100
pore width (nm)

Fig. 7.

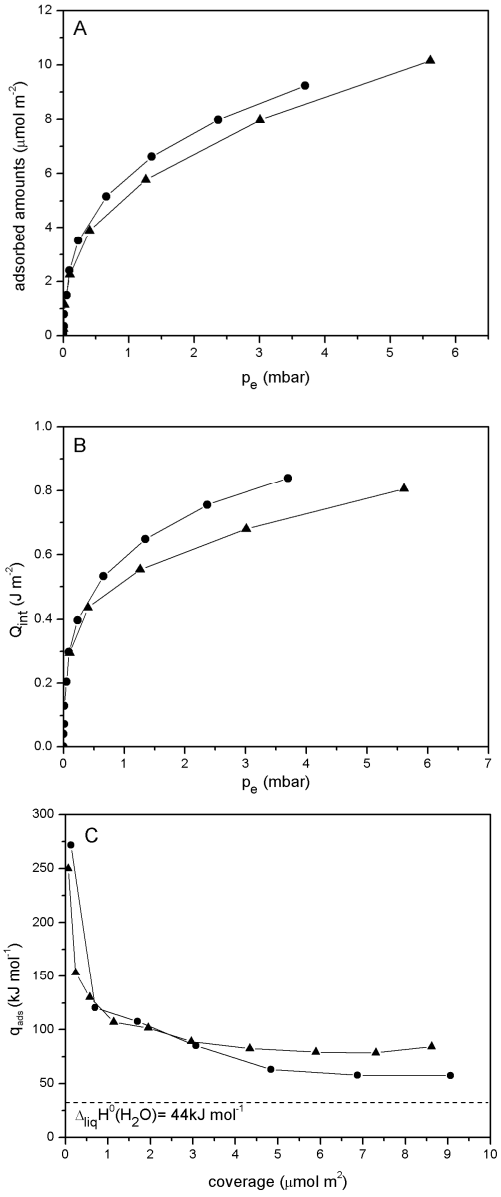
A
adsorbed amounts (μmol m-2)
pe (mbar)
B
Qint (J m-2)
pe (mbar)
C
qads (kJ mol-1)
ΔliqH°(H2O)= 44kJ mol-1
coverage (μmol m2)

Fig. 8.

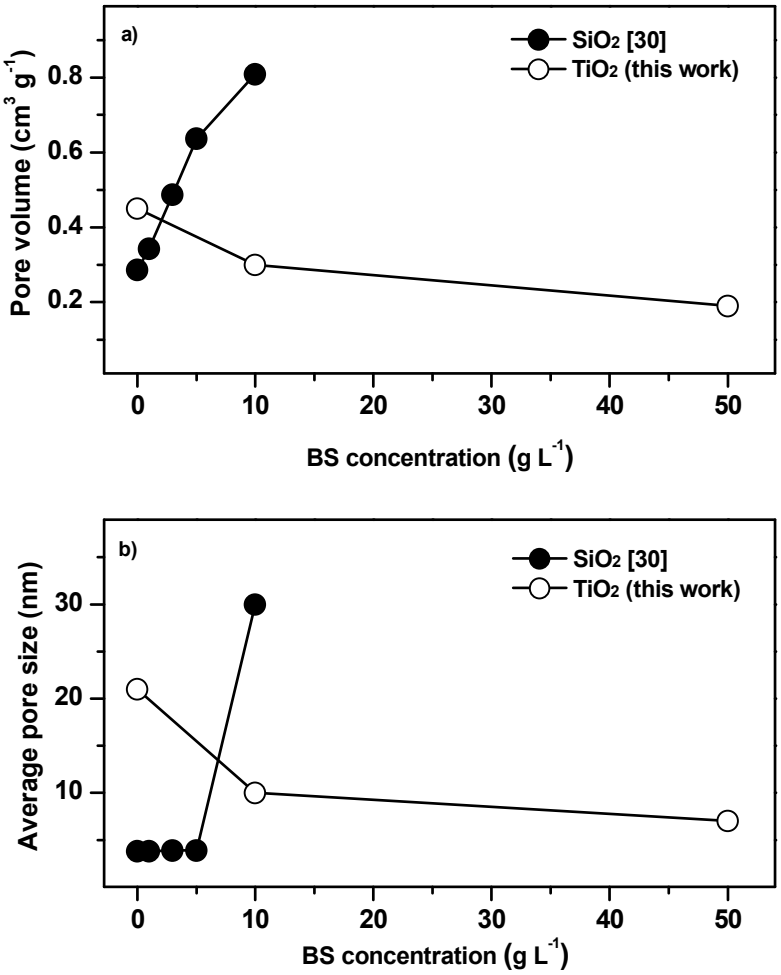
a)
SiO2 [30]
TiO2 (this work)
Pore volume (cm3 g-1)
0.2
0.4
0.6
0.8
0
10
20
30
40
50
BS concentration (g L-1)
b)
SiO2 [30]
TiO2 (this work)
Average pore size (nm)
10
20
30
0
10
20
30
40
50
BS concentration (g L-1)

Fig. 9.

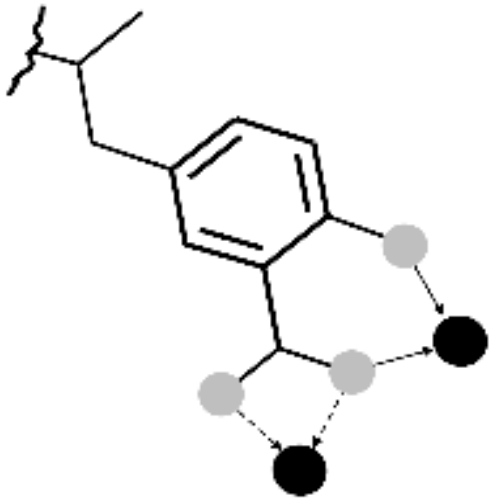

Fig. 10.